AURORAL DIAGNOSTICS FOR POGOLITE ASTROPHYSICAL BALLOON

O. Jokiaho[1], N. Ivchenko[2], H. Dahlgren[3], D. Whiter[4], and M. Alaniz[5]

[1]*Department of Space Environment Physics, University of Southampton, UK, Email: opj100@phys.soton.ac.uk*
[2]*Space and Plasma Physics, Royal Institute of Technology, Stockholm, Sweden, Email: nickolay.ivchenko@ee.kth.se*
[3]*Space and Plasma Physics, Royal Institute of Technology, Stockholm, Sweden, Email: hanna.dahlgren@ee.kth.se*
[4]*Department of Space Environment Physics, University of Southampton, UK, Email: d.k.whiter@phys.soton.ac.uk*
[5]*Space and Plasma Physics, Royal Institute of Technology, Stockholm, Sweden, Email: alaniz_monica@hotmail.com*

ABSTRACT

The PoGOLite balloon experiment, to be launched from Kiruna in August 2010 will investigate polarisation of X-rays from astrophysical objects. Auroral emissions in the measured wavelength range enhance the background level for the experiment, but also constitute an interesting object of their own. The state-of-the art PoGOLite instrument will benefit from careful characterisation of aurora, and could provide unique results on the auroral X-ray polarisation.

We present the design of the auroral diagnostic package to be flown onboard the PoGOLite balloon. It consists of two photometers and a fluxgate magnetometer. The photometers are equipped with Fabry-Perot etalons, which are scanned in wavelength by tilting, to measure auroral emissions as well as the surrounding background. The fluxgate magnetometer will characterize the auroral electrojet currents (to put observations in context of the sub-storm dynamics), and low frequency waves, which are thought to be responsible for pitch-angle diffusion of trapped high energy electrons.

1. INTRODUCTION

PoGOLite is an astrophysical balloon experiment to study the spectrum, flux, occurrence, variability and polarisation of X-rays from the Crab Nebula (R.A. = $05^h34^m32^s$, Dec = $+22°00'52''$) and Cyg X-1 (R.A. = $19^h58^m22^s$, Dec = $35°12'06''$) in the energy range 20-80 keV. The balloon will first fly in August 2010 from Esrange, Sweden. To characterise the auroral situation during the flight, a combination of balloon-borne and ground based experiments will be used. On the ground radar and riometer techniques are used to support the magnetometer and a photometer assembly onboard.

This paper describes design features of the photometer assembly. Two narrow band auroral photometers equipped with tilting Fabry-Perot etalons will scan through a selected wavelength interval to measure the auroral events during the flight.

2. AURORAL X-RAYS

Auroral emissions in the X-ray range are well known. The main contributing mechanism at energies above several keV is the bremsstrahlung emitted by energetic electrons passing close to nuclei of atmospheric atoms. An electron has a finite probability of emitting X-rays with energy up to its initial energy. The cross-section of this process is however very small. Bremsstrahlung emission is excited by electron precipitation only. Energetic ions have been suggested to excite inner shell lines in charge exchange processes [1]. However, these emissions are only observable from satellites, and are absorbed at balloon altitudes.

For the energy range where PoGOLite detectors are sensitive, there are two statistical occurrence maxima. One is located close to magnetic midnight, and is related to substorm breakup. A recent paper [2] demonstrated X ray observations from the Polar satellite of a bright spot associated with the reconnection simultaneously seen in the magnetotail by Cluster satellites. Such strong and dynamic aurora will clearly affect the background in the PoGOLite observations. The intensities have been compared to typical astrophysical intensities in [3] which established the need for auroral diagnostics onboard the balloon.

The second maximum in auroral X ray emissions is observed in the morning sector. Analysis of the temporal evolution of the global emission pattern, done by [4] strongly suggests that the emissions are caused by electron precipitation from the population injected in the course of a substorm. As electrons drift eastward in the Earth magnetosphere, due to gradient-curvature drift, they are scattered into the loss cone and cause X ray emissions in a region progressing to the east with time passed after the injection.

Finally, one should mention X ray emissions excited

Proc. '19th ESA Symposium on European Rocket and Balloon Programmes and Related Research, Bad Reichenhall, Germany, 7–11 June 2009 (ESA SP-671, September 2009)

by precipitating relativistic electrons. These so called "Kiruna" events [5] exhibit spectra reaching above 1 MeV and are predominantly seen in the evening sector. They are thought to be related to scattering of trapped electrons from the radiation belts by means of interaction with Electro-Magnetic Ion Cyclotron (EMIC) waves.

3. CHOICE OF EMISSIONS

Even though the balloon is above the bulk of the atmosphere, scattering of the solar radiation is significant and greatly affects the design. The solar spectrum peaks at about 500nm. Additionally, due to Rayleigh scattering shorter wavelengths scatter more than longer wavelengths. Background light levels are greatest at sea level where scattering is greatest, but decreases fast with altitude. At the balloon altitude this can be up to several orders of magnitude making photometric observations of daytime aurora possible.

Therefore, clean auroral lines as far towards the red end of the optical spectrum as possible are preferred to our purposes. The fact that there are no photometer units readily available operating beyond the wavelength of 850 nm adds a further constraint. The atomic oxygen lines at 844.6 nm and 777.4 nm are sufficiently bright and relatively free from contamination. These spectral regions also include lines from the molecular N_2 first positive and N_2^+ Meinel bands in close approximity. Using a narrow bandwidth in bright background conditions, atomic lines are more readily resolved than the rotational spectra from molecular bands.

The atomic oxygen emission lines at 844.6 nm and 777.4 nm appear strong in aurora as well as in dayglow [6]. The only excitation method of significance is electron impact. In normal aurora this is provided by electron precipitation, at dayglow via photo-electrons as well as intermittent auroral electrons. Additionally, in daytime conditions a close co-incidence exists between the emission line of OI at 102.6 nm shown in Fig. 1 and the solar EUV Lyβ emission line at 102.6 nm in Fig. 2 known as the Bowen fluorescence [7]. This leads to an increase in the OI 844.6 nm brightness. The 777.4 nm is unaffected as there is no resonant line feeding to it. As both of these emission are triplet lines, these excitation mechanisms do not only affect the integrated intensity but also the relative triplet line strengths via oscillator strengths.

The brightness of the 844.6 nm and 777.4 nm lines have been reported in both twilight and dayglow. Early airglow intensities for the 844.6 nm emission were calculated by [10]. It was found that the total dayglow would be about 500 R and the twilight intensity in the order of 1 R. Later daytime intensities have been reported as 1 kR [6]. Observed intensities of 1.1 kR for 844.6 nm and 1.6 kR for 777.4 nm have been observed [11]. Twilight intensities of 844.6 nm have also been reported by [12] of about 13 R.

More recently, the twilight intensity decay of the

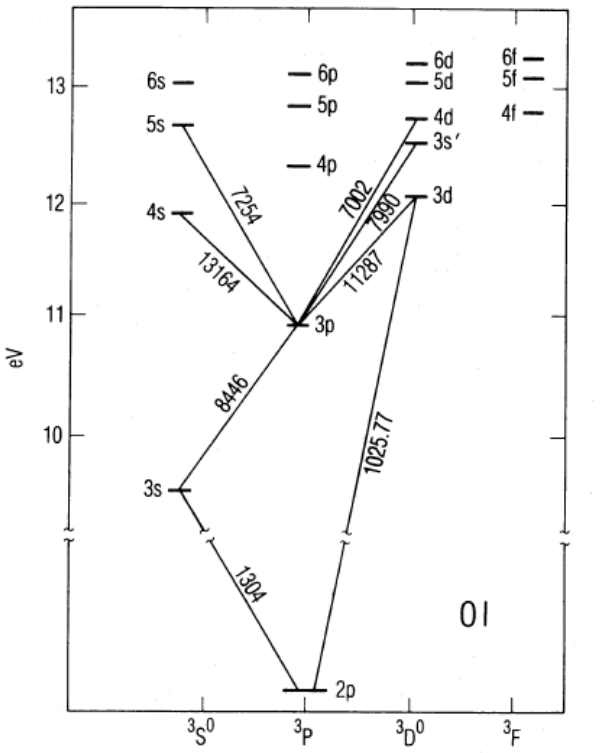

Figure 1. Energy level diagram of OI 844.6 nm.[8]

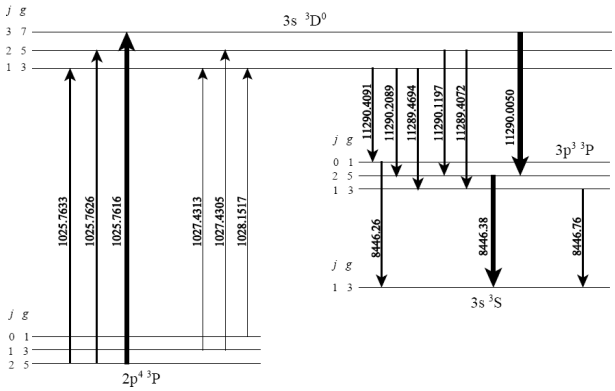

Figure 2. The primary path of Bowen fluorescence in OI 844.6 nm emission. [9]

844.6 nm as a function of solar depression angle has been determined [13]. The relative triplet line strengths were also studied to determine the primary excitation mechanism between photoelectrons and solar resonance. The ratio between the lines (844.626 nm + 844.638 nm) / 844.676 nm was found to change by 0.13 $\pm$ 0.03 per degree of solar depression angle. They concluded that the Bowen cascade is not the primary excitation mechanism over photo-ionisation during twilight conditions. Airglow measurements provide a direct measure of the thermospheric oxygen concentration. Predicted average auroral intensity for 777.4 nm is 9.6 kR and for 844.6 nm 11.5 kR [14].

A bandwidth less than 0.01 nm would allow direct measurement of the solar resonance of 844.6 nm and photoelectron excitation and relative and absolute intensities of the triplet lines of both 777.4 nm and 844.6 nm. These depend on the excitation conditions, with and without aurora in both daytime and twilight conditions and we can simultaneously correlate and model the corresponding X ray production.

The background spectral intensity of atmospheric scattering for the duration of the flight is quantified with Modtran4. This directly affects the required filter bandwidth. Fig. 3 shows the results over a period of 24h after launch for the two target look directions of Crab and Cygnus X as well as the magnetic zenith from the observing altitude at one hour steps for two range of wavelengths: 768.9-781.5 nm and 840.3-850.3 nm.

Based on these results, the background level will be in the range of 10^4 R/Å. The auroral line intensities are around 10^2-10^3 R. Therefore, a resolution of better than 0.1 nm is needed for the filter bandwidth, only achievable with a Fabry-Perot etalon.

4. OPTICAL DESIGN

For the design of the photometer, we use a simple optical scheme, where the light passes through the filter system consisting of a Fabry-Perot etalon (FPE), and a narrow passband interference filter to select a single transmission peak of the FPE. The fore lens produces the image in its focal plane, where the field stop is located. After the field stop, the field lens images the entrance pupil (in this case given by the fore lens) onto the sensitive area of the Photomultiplying Tube (PMT). This assures the independence of the measured brightness on the details of the field illumination and sensitivity variation across the PMT.

The central wavelength (CWL) of the FPE passband depends on its physical dimensions, and the angle of incidence. For non-perpendicular incidence, the CWL shifts to the blue, with the shift proportional to the square of the angle of incidence (referred to the normal). This makes it possible to scan across a narrow range of wavelength by tilting the FPE. However, the CWL dependence on angle

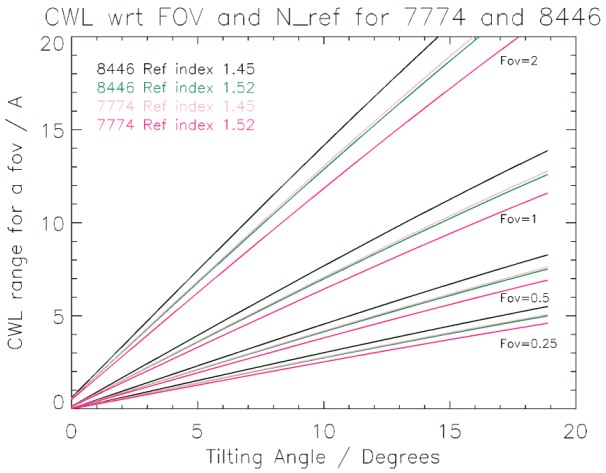

Figure 4. Spread of the central wavelength as a function of tilt angle and field of view for 777.4 nm and 844.6 nm for the refractive indices 1.44 and 1.52.

of incidence also sets the limitation on the field of view (as the passband varies across the field of view).

Improving the spectral resolution of the FPE (given by the width of the passband) quickly reduces the throughput of the system, as the field of view should decrease to keep the spread in the CWL across the field of view less than the FPE passband. This is illustrated in Fig. 4.

A Fabry-Perot etalon with a tilting mechanism up to a few degrees will be used to blue shift the central wavelength. The successive transmission maxima will be absorbed by a static interference filter with a bandpass of approximately the free spectral range of the etalon. Bright background conditions set the target FWHM for the etalon to a maximum of 0.5 Å. For a reasonable spatial scanning range and to limit the cost of the interference filter the free spectral range should be in the order of 2 nm. This leads to a finesse requirement of 40. The thickness required by this arrangement and the mirror flatness is difficult to achieve for a simple solid etalon. On the other hand, a tunable etalon is more suitable, but can be very costly. Another alternative is air spaced etalons, but the effect of smearing will be worse due to its lower refractive index.

Aperture size with the focal length of the object plane determines the field of view. The photon counts in the PMT head depend on the overall transmittance of the instrument, PMT efficiency and the geometric factor of the optics that depend on the field of view and light collecting area of the optics. The first two have been estimated as 0.1. Fig. 5 shows the number counts of photons per Rayleigh as a function of light collecting diameter and field of view. Secondly, the background counts have to be estimated. This is seen in Fig. 6. A scenario with a background level of 10^4 R/Å is used. Overall, the ratio seen in Fig. 7 can be achieved.

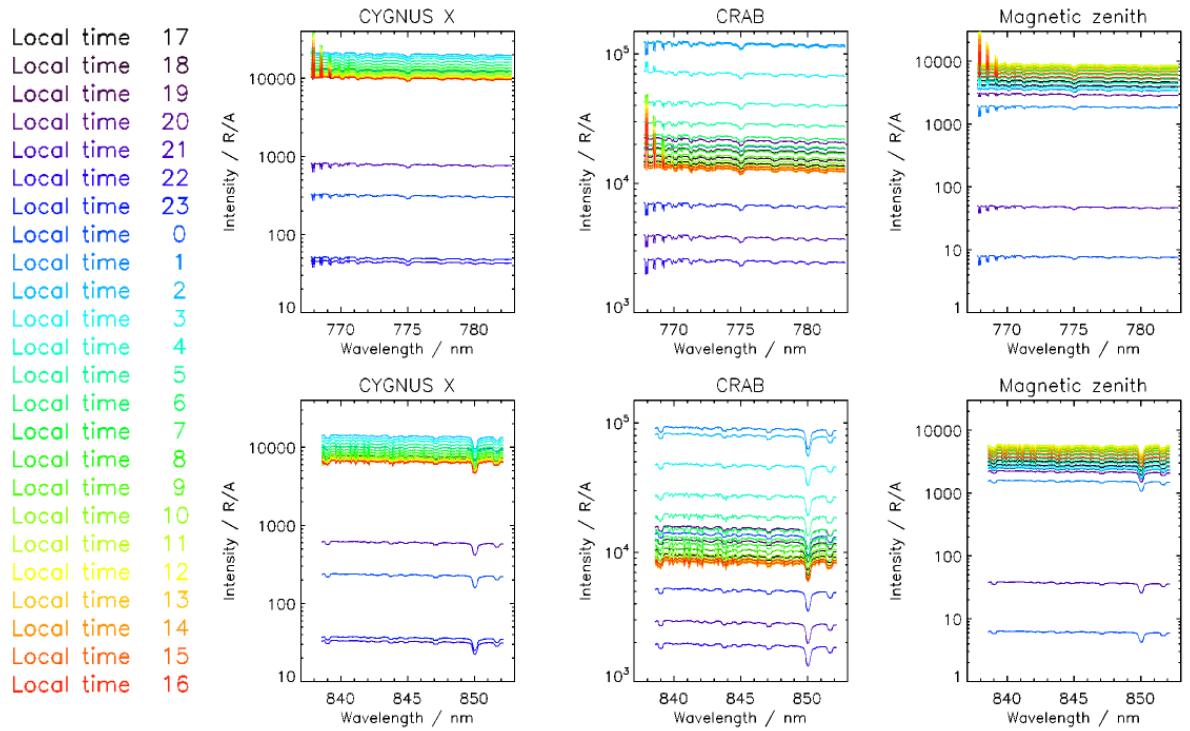

Figure 3. Theoretical sky background levels from the Modtran4 atmospheric model for the two target look directions as well as magnetic zenith for comparison.

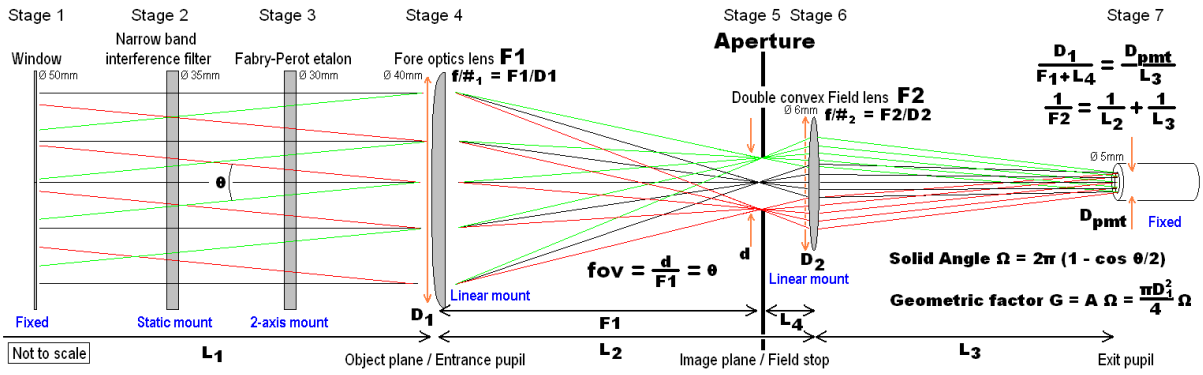

Figure 8. Optical layout. The values of the quantities are listed in Tab. 1.

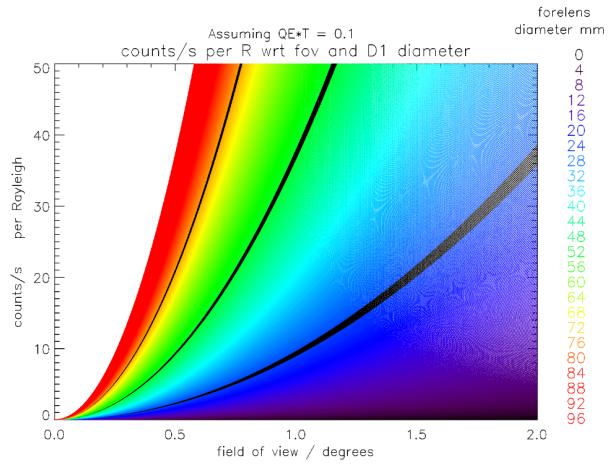

Figure 5. Number counts of photons per Rayleigh as a function of light collecting diameter and field of view on target lines of aurora. Diameters of 25, 50 and 75 mm are highlighted in black.

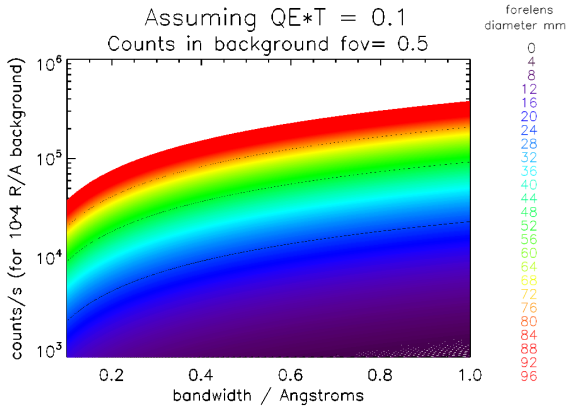

Figure 6. Photon counts for a background level of 10^4 R/Å as a function of the Fabry-Perot etalon bandwidth and light collecting diameter. Field of view is 0.5 degrees.

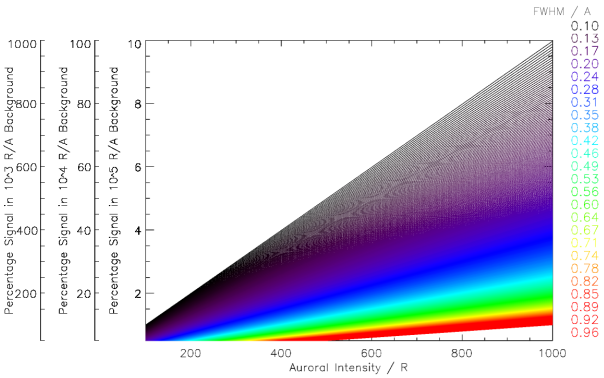

Figure 7. Ratio between counts per second produced from aurora 100-1000 R and by background levels of 10^3, 10^4 and 10^5 R/Å.

5. FINAL DESIGN

Table 1. Optical layout quantities, defined in Fig. 8.

D1 (mm)	F1 (mm)	L2 (mm)	L3 (mm)	L4 (mm)	L5 (mm)
40.0	200.0	210.0	35.0	10.0	45.0

A sketch of the optical design is seen in Fig. 8. The first stage of the optical system includes a window 40 mm in diameter with an antireflection coating through which the light enters the detector. The second stage consists of a narrow bandpass interference image quality filter of 35 mm in diameter, 1.7 nm in full width at half maximum, and centered at 777.3 nm and 844.5 nm respectively for the two photometers (Tab. 2). These are fitted into a static mount.

The third stage involves a solid Fabry-Perot etalon of 30 mm in diameter which is fixed into a square filter holder. This is attached to a two axis square filter mount, where one axis is manually adjusted and the other by a miniature motorised piezo electric actuator to allow tilting of the filter to scan in wavelength. The etalon is characterised by a finesse of about 40, free spectral range of 1.9 nm and full width at half maximum of less than 0.05 nm (Tab. 3). The two etalons are centered at wavelengths of 777.6 nm and 844.8 nm respectively.

The fourth stage is the fore-optics which incorporates an achromatic doublet lens to reduce spherical aberrations. The lens is 40 mm in diameter with a focal length of 200 mm and f/4.8 mounted onto a manually focusing linear micro positioning stage that allows adjustments to be made on the location of the lens with respect to the image plane at the field stop (fifth stage).

Similarly, the field lens which forms the sixth stage is a double convex lens 6 mm in diameter, 30 mm in focal length with f/5.0. The lens is attached to a linear micro positioning stage that allows the image of the forelens to be projected onto the PMT unit (stage 7). The lenses and filters are antireflection coated apart from the Fabry-Perot etalon and the field lens. The components are attached to an optical bench that is fitted into a cylindrical aluminum container with one photometer on each side. Total length of the optical system is 549 mm allowing 150 mm between stage one and stage four. The distance between stage four and stage six is 210 mm, 35 mm between stage six and seven and further 154 mm is reserved for the PMT and cabling.

The application requires PMT modules sensitive towards the near infrared region with reasonable quantum efficiency. Photon counting GaAs PMT modules H7421-50 by Hamamatsu are used , which incorporate a PMT tube, a high-voltage power supply circuit, a voltage-divider circuit and a photon counting discriminator circuit. They provide peak cathode sensitivity of 90 mA/W at 800 nm and quantum efficiency at 12% at peak sensitivity. Manufacturer indicates dark counts of 100 per second. The

Table 2. Optical parameters

	Ø (mm)	CWL (nm)	FWHM (nm)	T	optical density
Interference	35.0	777.3	1.70	60%	5
filter	35.0	844.5	1.70	60%	5

Table 3. Optical parameters

	Ø (mm)	CWL (nm)	FWHM (nm)	FSR (nm)	d (μm)	F	T	R
Solid	30.0	777.6	<0.05	1.9nm	104±1	40	70%	93%
etalon	30.0	844.8	<0.05	1.9nm	123±1	40	70%	93%

counts are taken care of by a field-programmable gate array (FPGA), which also controls the tilting of the FPE.

Thermal aspects of the design (the need of a stable ambient temperature for stability of the CWL of the filters), and the high voltage supply in the PMT assembly mean that the optical system needs to be placed in a pressurised compartment.

6. SUMMARY

To be able to related the background in the PoGOLite observations to the auroral situation, one needs to characterize energetic electron precipitation. There is no unambiguous way of doing this, hence a strategy of combining multiple observational parameters is needed. To put the data in geophysical context, a fluxgate magnetometer will be placed onboard the balloon, for measuring the electroject strength, and the presence of EMIC waves. The magnetometer is SMILE (Small Magnetometer In Low mass Experiment), developed at KTH and LCISR [15]. A miniature sensor (20×20×20 mm cube) is coupled in digital processing loop, where the correlation is implemented with the known response to a given field change. Ground based techniques for observing the ionosphere (such as incoherent scatter radar, ionosonde, and riometer) are all sensitive to energetic precipitation producing ionisation in the lower E and D regions. These techniques are equally sensitive to energetic ion and electron precipitation, while the former will not produce observable X ray emissions.

Precipitation of auroral electrons with energies of tens of keV is readily observed by optical mean, allowing the highest possible time resolution. However, the bright sky background presents an observational challenge for the simple concept of auroral photometer recoding the sky brightness in an auroral emission. Minimising the effect of the background (due to solar scattering in the upper atmosphere) requires on one hand accurate characterisation of the background, and on the other hand careful selection of the emission. Choice of atomic lines in the near-infrared provides a good combination of low background, detector sensitivity and narrow line width. Use of a low Fabry-Perot etalon with narrow passband interference filter allows to construct a spectrometer with a passband of about 0.05 nm. The central wavelength can be scanned by means of tilting the Fabry-Perot Etalons.

The launch from Kiruna in August, near the turning of the high altitude winds, warrants controlled location of the balloon above northern Scandinavia. Ground based data, collected from this area will be used together with the balloon-borne instruments, to validate their observation, which is necessary for the long duration balloon flight envisioned for PoGOLite in the future.

REFERENCES

[1] Bhardwaj, A., 2007, J. Atmos. Sol-terr. Phy., 69, 179187

[2] Borg, A. L., 2007, J. Geophys. Res., 112, A06215, 2007

[3] Larsson, S., Ryde, F., Ivchenko, N., Pearce, M., ESA-SP-647, ESAPAC Proceedings, Visby, Sweden, 2007

[4] Østgaard, N., 2000, J. Atmos. Sol-terr. Phy., 62, 889

[5] Millan, R. M., 2002, J. Geophys. Res., 29, 24, 2194

[6] Dalgano, A., 1969, Phil. Trans. R. Soc. Lond., 264, 153-160

[7] Bowen, I. S., 1947, Publ. Astron. Soc. Pacific, 59, 196

[8] Rudy, R. J., Rossano, G. S., Puetter, R. C., 1989, Astrophys. J. , 346, 799-802

[9] Watchorn, S., Noto, J., Waldrop, L. S., Migliozzi, M. A., 2007, Proc. SPIE, 6689

[10] Brandt, J. C., 1959, Astrophys. J., 130, 228

[11] Vallance Jones, A., 1973, Space Sci. Rev., 15, 355-400, 392

[12] Shefov, N. N., 1962, Serija Rezul'taty MGG, 9, 55

[13] Lancaster, R. S., Kerr, R. B., Ng, K., Noto, J., Franco, M., Solomon, S. C., 1994, Geophys. Res. Lett., 21, 829-832

[14] Vallance Jones, A., 1974,D. Reidel Publishing Company, Dordrecht, 1974.

[15] Forslund, Å., Belyayev, S., Ivchenko, N., Olsson, G., Edberg, T., Marusenkov, A., 2007, Meas. Sci. Technol., 19, 015202